



OPEN

# Lewis acid-mediated Suzuki–Miyaura cross-coupling reaction

Takashi Niwa<sup>1,6</sup>, Yuta Uetake<sup>2,3</sup>, Motoyuki Isoda<sup>1,7</sup>, Tadashi Takimoto<sup>1</sup>, Miki Nakaoka<sup>1</sup>, Daisuke Hashizume<sup>4</sup>, Hidehiro Sakurai<sup>2,3</sup> and Takamitsu Hosoya<sup>1,5</sup>

**The palladium-catalysed Suzuki–Miyaura cross-coupling reaction of organohalides and organoborons is a reliable method for carbon–carbon bond formation. This reaction involves a base-mediated transmetalation process, but the presence of a base also promotes competitive protodeborylation. Herein, we established a Suzuki–Miyaura cross-coupling reaction via Lewis acid-mediated transmetalation of an organopalladium(II) intermediate with organoborons. Experimental and theoretical investigations indicate that the controlled release of the transmetalation-active intermediate enables base-independent transmetalation under heating conditions and enhances the applicable scope of this process. This system enables us to avoid the addition of a traditional base and, thus, renders substrates with base-sensitive moieties available. Results from this research further expand the overall utility of cross-coupling chemistry.**

The Suzuki–Miyaura cross-coupling (SMC) reaction is one of the reliable carbon–carbon bond forming processes, broadly applied in the synthesis of valuable compounds, such as pharmaceuticals<sup>1,2</sup>. A critical step in the SMC reaction is the transmetalation of organopalladium(II) species with organoborons, which conventionally requires the use of a base<sup>3</sup>. Basic conditions, however, also occasionally cause undesired protodeborylation, particularly when using industrially valuable organoborons, such as perfluoroaryl- and heteroarylborons (Fig. 1a)<sup>4,5</sup>. This issue has been recognized as the base problem<sup>6</sup>, and therefore, numerous efforts have been devoted to suppressing the side reaction and broadening the range of synthetically available chemical structures<sup>7,8</sup>. A straightforward approach to solving this problem is to avoid the addition of a base. Indeed, the SMC reaction has been shown to proceed without a base under exceptional conditions (for example, employing specific substrates). For example, transmetalation can occur with organo(trialkoxo) borates without an additional base because of their high nucleophilicity<sup>9,10</sup>. Sanford et al. have recently reported that the use of acyl fluorides as electrophiles allows for a nickel-catalysed SMC reaction with organoboronic acids without using an exogenous base, in which the fluoride within the substrates promotes transmetalation<sup>11</sup>. The SMC reaction is also known to occur without a base or heating when aryldiazonium salts are employed as electrophiles, in which the transmetalation of coordinatively unsaturated cationic arylpalladium(II) with organoboronic acids proceeds (Fig. 1b)<sup>12–15</sup>. These pioneering studies have solved the base problem by substrate design. Herein, we report a strategy to avoid the addition of a traditional base to the SMC reaction of readily available organohalides with organoborons enabled by the design of catalytic intermediates.

## Results

**Initial considerations.** We took inspiration from the reactivity of aryl-diazonium salts, which indicates that cationic organopalladium(II)

species can help develop a traditional base-free SMC reaction (Fig. 1b). A challenge in realizing this approach is the overcoming of the thermal instability of the cationic arylpalladium(II) species, which limits the reaction temperature<sup>13</sup>. Indeed, only an aryldiazonium salt can react with a palladium catalyst at room temperature to generate a cationic arylpalladium(II) complex via oxidative addition and releasing the dinitrogen, avoiding the necessity of heating. Since SMC reactions often require heating to complete a catalytic cycle, preventing the thermal decomposition of palladium intermediates is indispensable for the generalization of the traditional base-free methodology for carbon–carbon bond formation.

To address this issue, we designed a coordinatively saturated cationic organopalladium(II) intermediate with labile ligands that are thermally stable and release the corresponding unsaturated and transmetalation-active species in equilibrium (Fig. 1c). The controlled release of cationic organopalladium(II) species should suppress the spontaneous degradation and prioritize the desired pathway even under heating conditions. We envisioned that this masked intermediate can be generated via the dehalogenation of an aryl(halo)palladium(II) complex with a halophilic Lewis acid, where the thus-formed metal halides serve as labile ligands. Conventionally, dehalogenation often employs silver(I) salts, which are unsuitable for this approach because of their redox activities that terminate the catalytic cycle via the oxidation of palladium(0) species. The low solubility of silver(I) halides in organic solvents is also problematic, because they precipitate out without serving as ligands. Hence, our investigation commenced with exploration of Lewis acids that are suitable for our purpose.

**Optimization of reaction conditions.** To verify our hypothesis, various halophilic metal salts were screened for the SMC reaction between aryl bromide **1** and a small excess of potassium phenyl(trifluoro)borate **2a** (ref. 16) in the presence of PdCl<sub>2</sub>(amphos)<sub>2</sub>

<sup>1</sup>Laboratory for Chemical Biology, RIKEN Center for Biosystems Dynamics Research (BDR), Kobe, Hyogo, Japan. <sup>2</sup>Division of Applied Chemistry, Graduate School of Engineering, Osaka University, Suita, Osaka, Japan. <sup>3</sup>Innovative Catalysis Science Division, Institute for Open and Transdisciplinary Research Initiatives (ICS-OTRI), Osaka University, Suita, Osaka, Japan. <sup>4</sup>RIKEN Center for Emergent Matter Science (CEMS), Wako, Saitama, Japan. <sup>5</sup>Laboratory of Chemical Bioscience, Institute of Biomaterials and Bioengineering, Tokyo Medical and Dental University (TMDU), Tokyo, Japan. <sup>6</sup>Present address: Laboratory of Chemical Bioscience, Institute of Biomaterials and Bioengineering, Tokyo Medical and Dental University (TMDU), Tokyo, Japan. <sup>7</sup>Present address: Department of Pharmaceutical Sciences, School of Pharmacy at Fukuoka, International University of Health and Welfare, Okawa, Fukuoka, Japan. ✉e-mail: [takashi.niwa@riken.jp](mailto:takashi.niwa@riken.jp); [uetake@chem.eng.osaka-u.ac.jp](mailto:uetake@chem.eng.osaka-u.ac.jp)

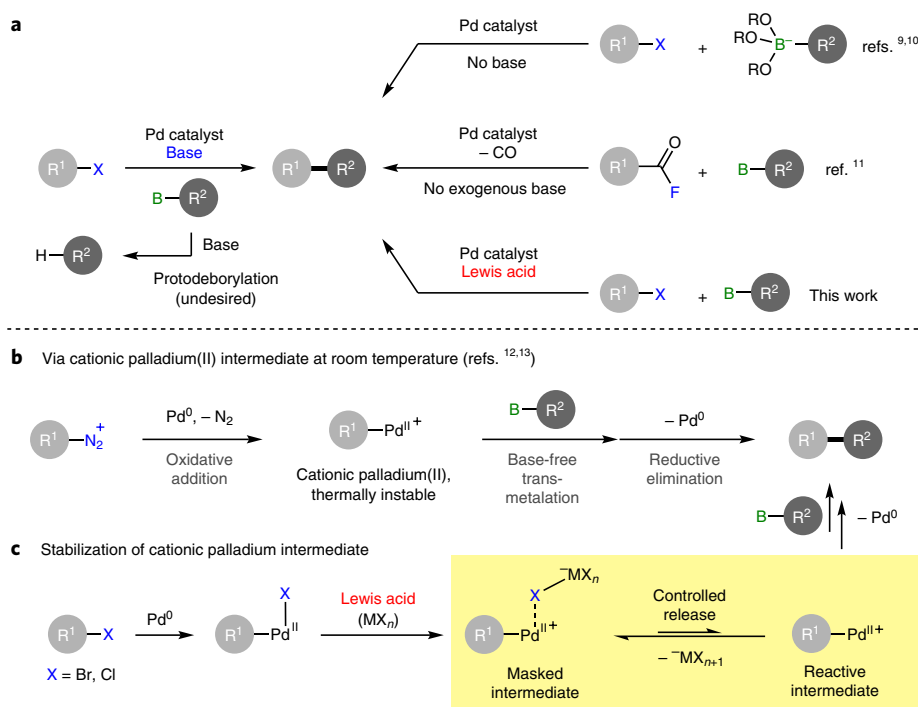


**Fig. 1 | SMC reactions.** **a**, Schemes of SMC reactions with or without using an external base. **b**, SMC reaction with aryldiazonium salts as electrophiles via the formation of a cationic arylpalladium(II) intermediate. **c**, Working hypothesis of a Lewis acid-mediated SMC reaction with organohalides via the controlled release of a cationic arylpalladium(II) intermediate. R, substituent; X, leaving group, unless otherwise noted; B, boryl group.

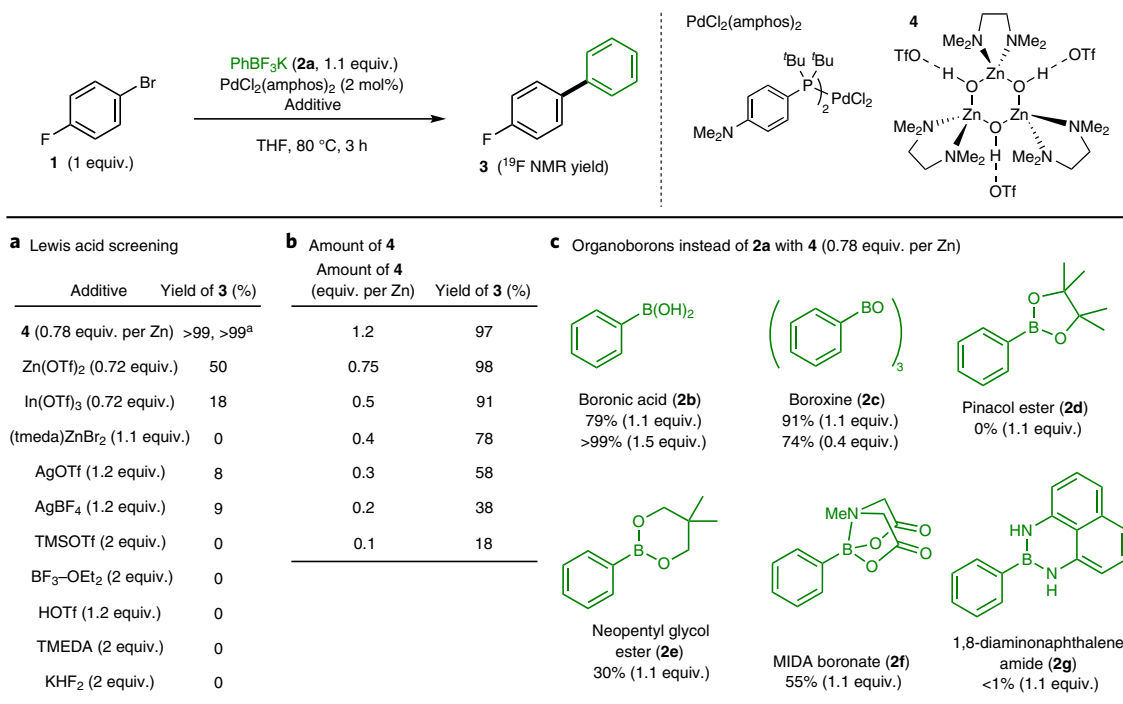


**Fig. 2 | Lewis acid-mediated SMC reaction.** The reaction scheme is shown at the top. Reaction conditions: **1** (0.20 mmol, 1 equiv.), **2** (0.22 mmol, 1.1 equiv., unless otherwise noted), PdCl<sub>2</sub>(amphos)<sub>2</sub> (4 μmol, 2 mol%), additive, THF (1 ml), under argon at 80 °C. Yields were determined by <sup>19</sup>F NMR with (trifluoromethyl)benzene as an internal standard. **a**, Optimization of additives. <sup>a</sup>The reaction was performed at room temperature for 24 h. **b**, Investigation of the amount of **4**. **c**, Scope of phenylboronic acid derivatives.

at 80 °C (amphos: di-*tert*-butyl(4-dimethylaminophenyl)phosphine). During this process, we found several metal triflates that provided 4-fluorobiphenyl (**3**; Fig. 2a and Supplementary

Table 2). Among them, a zinc trimer, that is, ((tmeda)Zn(OH)(OTf))<sub>3</sub> (**4**), easily prepared from zinc(II) triflate and *N,N,N',N'*-tetramethylethylenediamine (tmeda), demonstrated the best

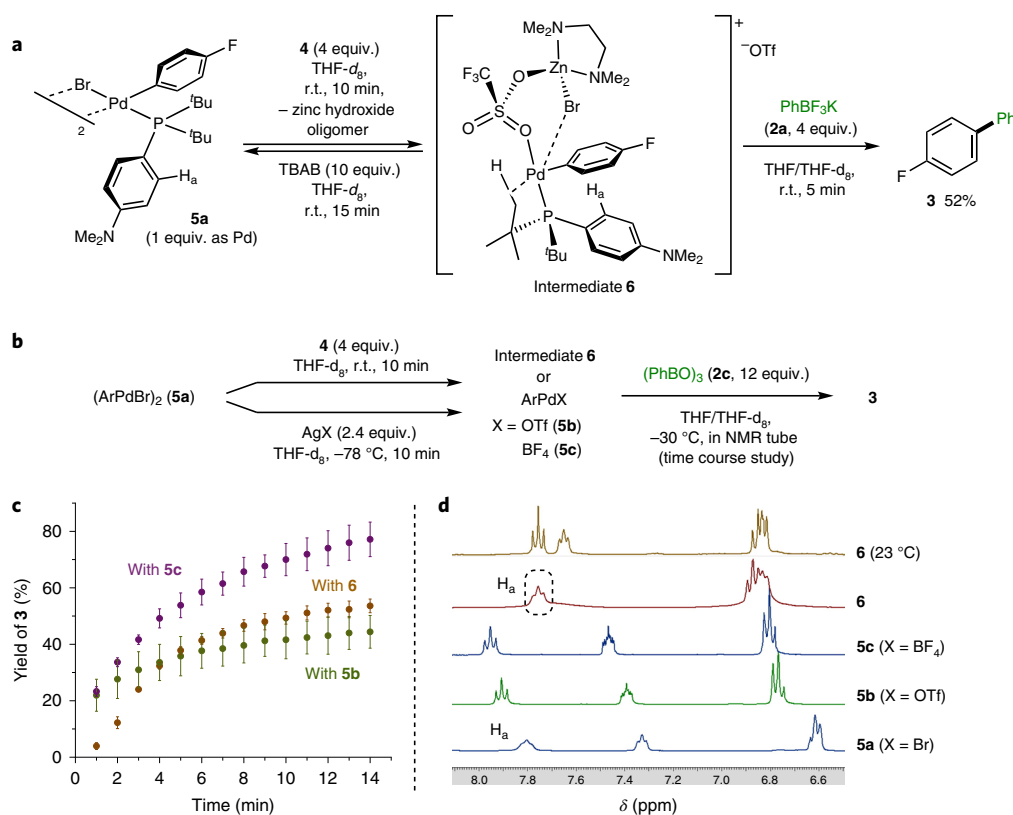


**Fig. 3 | Stoichiometric reactions.** **a**, Generation of intermediate **6** and its reaction with **2a**. For characterization of the chemical structure of intermediate **6**, see the following section in the main text. r.t., room temperature. **b**, Generation and reaction of **6** and the related cationic palladium complexes (**5b** and **5c**). **c**, Time-course plots of the yield of **3** in the reaction of **2c** with **5b**, **5c** and **6** at  $-30\text{ }^{\circ}\text{C}$ . The error bars mean the standard deviations calculated from three independent experiments for each complex. For detailed data, see Supplementary Tables 9–11. **d**, Enlarged view of  $^1\text{H}$  NMR spectra in the aromatic region ( $\delta$  8.1–6.5 ppm) of **5a–c** ( $-30\text{ }^{\circ}\text{C}$ ) and **6** ( $-30\text{ }^{\circ}\text{C}$  and  $23\text{ }^{\circ}\text{C}$ ). The chemical shift ( $\delta$ ) was corrected by setting that of the residual THF signal to 1.72 ppm.

result to afford **3** in quantitative yield. The use of indium(III) triflate also yielded **3**, while no conversion was observed when hard Lewis acids, such as boron trifluoride or trifluoromethanesulfonic acid (HOTf), were added, suggesting that the halophilicity of the additives is crucial. The addition of silver salts resulted in a low conversion, in agreement with our assumption. Heating was not essential: the reaction occurred even at room temperature to afford **3** in excellent yield. A precise investigation revealed that more than half of a zinc atom equivalent is essential for completing the reaction (Fig. 2b), indicating that the zinc centre is responsible for two catalytic cycles. This result suggests that the hydroxy group of **4** is not necessary for the transformation because it should be removed from **4** if it serves as a base in the first cycle and not be involved within the second cycle. A screening study of ligands for palladium catalysts showed that di- or tri(*tert*-butyl)phosphines, including amphos, were preferable, whereas di- or tricyclohexylphosphines yielded poor results (Supplementary Fig. 2). Other series of phenylboron derivatives, including phenylboronic acid (**2b**) and *N*-methyliminodiacetic acid (MIDA) derivative **2f** (ref. <sup>17</sup>), were applicable under these conditions, while the use of phenylboronic acid pinacol ester (**2d**) and phenyl(naphthalene-1,8-diamino)boron (**2g**)<sup>18</sup> did not afford the desired product, demonstrating the unconventional selectivity of boronic acid esters for SMC reactions (Fig. 2c).

**Stoichiometric reactions.** Stoichiometric reactions were conducted to confirm the role of the zinc complex. We synthesized aryl(bromo)palladium(II) dimer **5a** and fully characterized its structure by single crystal X-ray diffraction analysis (Supplementary Fig. 3). Nuclear magnetic resonance (NMR) spectroscopy revealed

that treatment of **5a** with four equivalents of **4** produced a new species (Fig. 3a and Supplementary Table 7), along with an insoluble zinc hydroxide oligomer (Supplementary Fig. 9). The regeneration of **5a** was observed by adding an excess amount of tetra(*n*-butyl) ammonium bromide (TBAB) to this mixture, indicating that this intermediate (**6**) formed via debromination by zinc complex **4** (Supplementary Table 8). Intermediate **6** showed notable reactivity to various phenylborons, as the reaction with several organoborons **2a–c** was completed within 5 min to afford **3**. The reactivity of **6** was compared with those of the related cationic palladium complexes (**5b** and **5c**), generated by the treatment of **5a** with silver salts (Fig. 3b). The reaction between each palladium intermediate and **2c**, a well-dissolvable organoboron derivative in tetrahydrofuran (THF), occurred even at  $-30\text{ }^{\circ}\text{C}$ . The reaction rate mediated by zinc complex **4** was comparable to that mediated by silver tetrafluoroborate ( $\text{AgBF}_4$ ), and higher than that mediated by silver triflate ( $\text{AgOTf}$ ) (Fig. 3c). By contrast, a substantial difference in stability was observed between the two groups. Namely, **6** remained unchanged for more than a day in  $\text{THF-}d_8$  at  $23\text{ }^{\circ}\text{C}$ , while the **5b** and **5c** smoothly decomposed at room temperature (Supplementary Figs. 4–6). These results indicate that **6** possesses both sufficient thermal stability and reactivity with organoborons owing to the presence of Zn species. The  $^1\text{H}$  NMR spectra of **6**, **5b** and **5c** demonstrated that almost all the signals in the aromatic region shifted to a low magnetic field, reflecting the electrophilically activated nature of each palladium centre (Fig. 3d). Meanwhile, the aromatic proton of **6** at the *ortho* position of the phosphine atom in the amphos ligand (corresponding to  $H_a$  of **5a** in Fig. 3a) was an intriguing exception, which showed a slightly higher magnetic field shift (Fig. 3d).

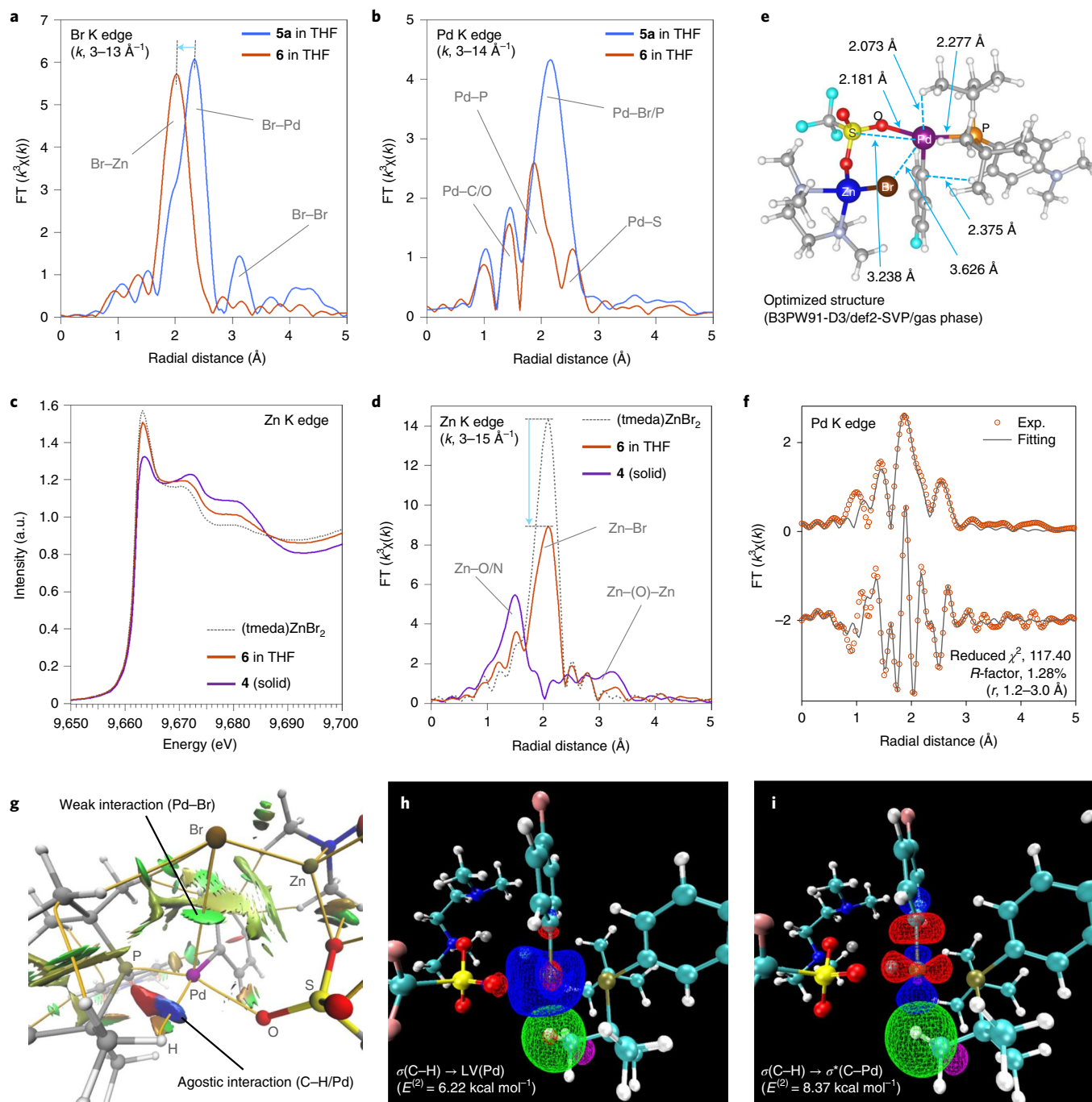


**Fig. 4 | XAS and electron density analyses of intermediate 6.** **a**, Br K-edge EXAFS. **b**, Pd K-edge EXAFS. **c**, Zn K-edge XANES. **d**, Zn K-edge EXAFS. FT, Fourier transformation;  $k$ , wavenumber ( $\text{\AA}^{-1}$ );  $\chi(k)$ , EXAFS oscillation. **e**, Reconstructed structure of **6** according to DFT calculation. **f**, Plots of the fitted curve for the Pd K-edge EXAFS in  $r$ -space: magnitude and its imaginary part. Exp., experimental. **g**, Isosurface of non-covalent interactions and bond paths obtained from quantum theory of atoms-in-molecules analysis. **h**, Reference orbitals in natural bond orbital basis representing  $\sigma(\text{C-H}) \rightarrow \text{LV}(\text{Pd})$  electron donation. LV, lone vacant. **i**, Reference orbitals in natural bond orbital basis representing  $\sigma(\text{C-H}) \rightarrow \sigma^*(\text{C-Pd})$  electron donation.

These observations illustrated the definite structural differences between **6** and the others.

**Characterization of the intermediate 6.** To elucidate the origin of the characteristics of intermediate **6**, structural analyses were conducted by X-ray absorption spectroscopy (XAS). We performed in situ XAS experiments of **6** formed by mixing **5a** and **4** in THF. In the Br K-edge extended X-ray absorption fine structure (EXAFS), the second peak ( $3.1 \text{ \AA}$ ) disappeared, and the first peak ( $2.3 \text{ \AA}$ )

shifted to the radial distance corresponding to the Br–Zn scattering ( $2.0 \text{ \AA}$ ; Fig. 4a). This result also revealed that the zinc complex **4** plays a role in the elimination of the bromine atom from the palladium centre. Pd K-edge EXAFS analysis of **6** indicated that, after the reaction, the singlet peak observed at the radial distance of  $2.2 \text{ \AA}$  was split into two peaks ( $2.0$  and  $2.6 \text{ \AA}$ ), attributed to the absence of bromine around the palladium centre (Fig. 4b). The second peak ( $2.0 \text{ \AA}$ ) was assigned to Pd–P bonding. The third peak ( $2.6 \text{ \AA}$ ) implied the presence of a relatively heavy element, which could be

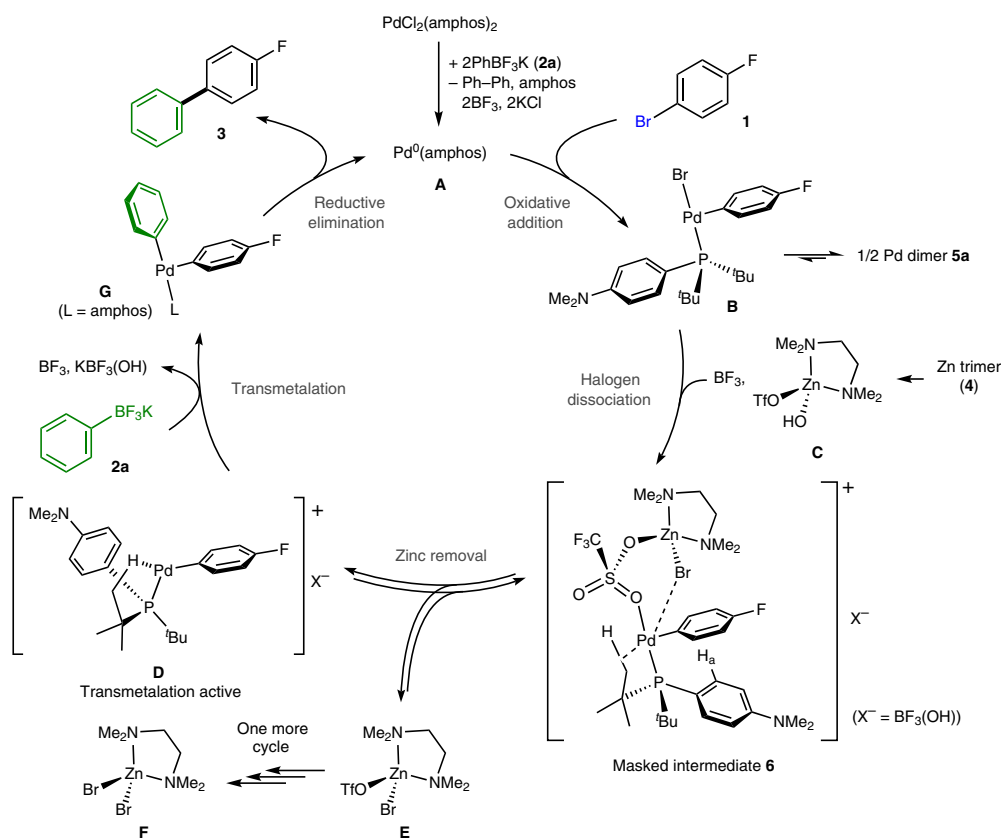


**Fig. 5 | Plausible mechanism.** A plausible mechanism is shown.  $H_a$  in intermediate **6** indicates the proton that showed the exceptionally high magnetic field shift of the peak observed in  $^1\text{H}$  NMR analysis (Fig. 3d).

assigned to the sulfur atom in triflate, indicating the formation of palladium triflate. Considering that the  $^1\text{H}$  NMR spectrum of the intermediate **6** was not identical to that of palladium triflate **5b** generated from  $\text{AgOTf}$  (Fig. 3d), we analysed the XAS data on the Zn K-edge in further detail. The X-ray absorption near edge structure (XANES) spectrum of **6** appeared to have intermediate features between those of the zinc complex **4** and  $(\text{tmeda})\text{ZnBr}_2$  (Fig. 4c). In addition, the lower peak intensity of **6** compared with the reference  $(\text{tmeda})\text{ZnBr}_2$  indicated that the coordination number of the bromine was one (Fig. 4d). These results suggest that zinc atom was connected with both bromine and oxygen atoms and that the local structure around zinc was  $\text{Br-Zn-O}$ . Based on our comprehensive analysis of XAS results, we proposed that the intermediate **6** in THF solution represents the formation of a Pd/Zn binuclear complex bridged by the triflate.

Based on the local structure derived from the XAS experiments, the entire structure was reconstructed using density functional theory (DFT) calculation at the B3PW91-D3/def2-SVP level of theory (Fig. 4e). Subsequently, the curve fitting of the Pd K-edge EXAFS of **6** was performed using the DFT-optimized structure as coordinates for calculating of scattering paths with the FEFF6 code<sup>19</sup>. The fitting results in  $r$ -space (1.2–3.0 Å) of the magnitude and imaginary part are plotted in Fig. 4f. The variations of all fitting parameters were within reasonable values, and the coefficient of multiple correlation ( $R$ ) factor was 1.28%, suggesting a good coincidence (Supplementary Table 14). The fitting confirmed that the third peak originated from the Pd–S scattering. In addition, the fittings of the EXAFS of **6** were performed on the Br K- and Zn K-edges as well (Supplementary Tables 13 and 15), and these results were also found to be consistent with the proposed structure. Overall, we conclude that the proposed triflate-bridged Pd/Zn binuclear complex is the most plausible

candidate for the intermediate. The plausibility of this structure was also supported by the peak shift observed in  $^1\text{H}$  NMR spectra to a higher magnetic field ( $H_a$  in Fig. 3d). Two-dimensional NMR and DFT analyses of **6** revealed that the aromatic proton  $H_a$  at the *ortho* position of the phosphine atom is directed towards the centre of the fluorophenyl group (Supplementary Fig. 17) and is therefore magnetically shielded. The estimated structure does not involve the hydroxy group of **4**, indicating that this group does not serve as a base to promote the subsequent transmetalation with organoborons (Supplementary Fig. 19). The observed formation of a zinc hydroxide oligomer as an insoluble by-product further supported our argument (Supplementary Fig. 9).

Based on the estimated structure of **6**, theoretical surveys were conducted to reveal the origin of the thermostability. The hydrogen atom of the *tert*-butyl group in the amphos ligand is located near the vacant coordination site of the palladium centre at the distance of 2.073 Å (Fig. 4e), which implies an agostic interaction. To gain information about electrostatic interactions, we analysed the non-covalent interactions<sup>20</sup> and identified a strong interaction between the palladium centre and the hydrogen atom of amphos (Fig. 4g, blue isosurface). The quantum theory of atoms-in-molecules<sup>21</sup> analysis also revealed the presence of a bond critical point between the palladium atom and the carbon–hydrogen bond with a relatively high electron density ( $\rho_{\text{bcp}}(r) = 0.250 \text{ e } \text{Å}^{-3}$ ) and a Wiberg bond index of 0.167, which indicates an agostic interaction (Supplementary Table 16). The donor-acceptor interaction energies ( $E^{(2)}$ ) calculated from the second-order perturbation theory analysis in natural bond orbital basis revealed electron donations from the  $\sigma(\text{C-H})$  orbital to the vacant Pd orbital ( $E^{(2)} = 6.22 \text{ kcal mol}^{-1}$ ) and  $\sigma^*(\text{C-Pd})$  orbital ( $E^{(2)} = 8.37 \text{ kcal mol}^{-1}$ ) (Fig. 4h,i). The natural bond orbital analysis indicated moderate electron donation (net  $E^{(2)} = 14.59 \text{ kcal mol}^{-1}$ )



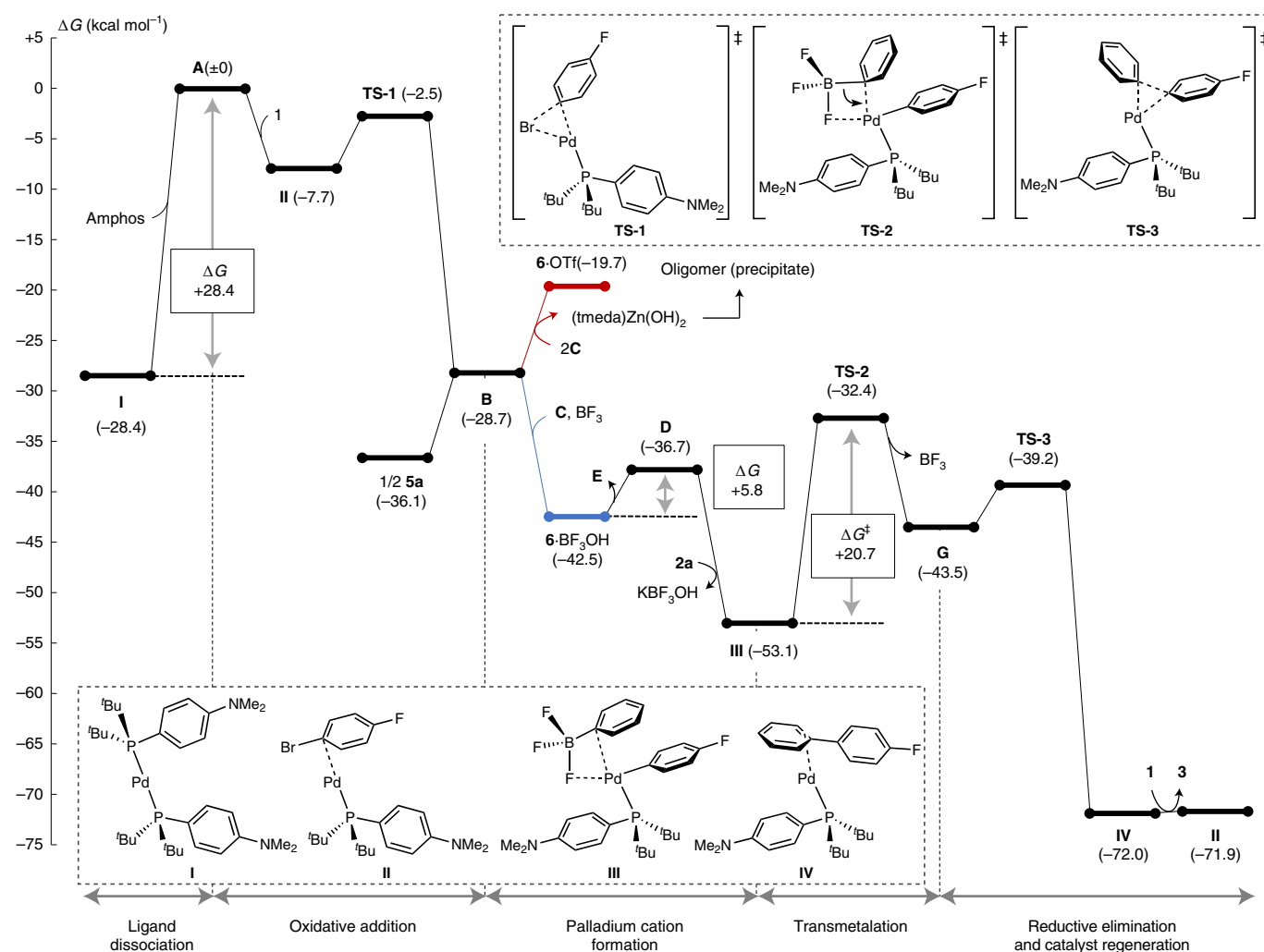


**Fig. 6 | DFT calculation study.** Energy profile of the zinc-mediated SMC reaction. The calculated Gibbs energies ( $\Delta G$  and  $\Delta G^\ddagger$ ; 298.15 K, 1 atm) are shown in kcal mol<sup>-1</sup>. The generation pathways from **B** for **6** under a stoichiometric condition (Fig. 3) and a catalytic condition are indicated by red and blue lines, respectively. For detailed profiles, see Supplementary Figs. 23–26.

from the  $\sigma(\text{C-H})$  orbital of the proximal *tert*-butyl groups to the cationic palladium centre. The broadening of *tert*-butyl group signals in the <sup>1</sup>H NMR spectra also indicates the presence of an agostic interaction between the palladium centre and the hydrogen atom (Supplementary Fig. 8). The separated proton signal was not observed even at low temperatures, suggesting the lability of the interaction. These results indicate that the carbon–hydrogen bond in the *tert*-butyl group serves as a hemilabile ligand and contributes to the high stability of intermediate **6**. The interaction would be crucial for the SMC reaction, because using a ligand that cannot form such an interaction (for example, dimethylphenylphosphine) resulted in a poor yield (Supplementary Figs. 2 and 27). We also identified a weak non-covalent interaction between the palladium centre and the eliminated bromine atom (Fig. 4g, green isosurface), which was supported by the low electron density value ( $\rho_{\text{bcp}}(r) = 0.060 \text{ e } \text{\AA}^{-3}$ ) and Wiberg bond index (0.091) at the bond critical point in the quantum theory of atoms-in-molecules analysis. This result suggests that the sterically hindered bromine atom at the remote apical position of palladium (Pd–Br, 3.626 Å) is loosely coordinated and enhances both the kinetic and thermodynamic stabilities of **6**.

**Reaction mechanism.** We proposed a mechanism for the zinc-mediated SMC reaction (Fig. 5). The reaction commences

with the reduction of the palladium(II) precursor with potassium phenyl(trifluoro)borate (**2a**) to afford coordinatively unsaturated mono(amphos)palladium(0) **A**. The oxidative addition of **1** provides arylpalladium(II) bromide **B**, which exists mainly as dimer **5a**. Then, the debromination by the zinc monomer (**C**), generated from **4**, affords the bimetallic intermediate (**6**), in which boron trifluoride, formed in the transmetalation, is assumed to capture the hydroxy group of **C**. We estimate that **6** is coordinatively saturated with a square planar structure and is therefore unavailable for direct transmetalation. The removal of the zinc moiety provides coordinatively unsaturated cationic complex **D**, which reacts with **2a** to give diarylpalladium(II) **G**. Finally, the reductive elimination of biaryl **3** regenerates **A** to complete the catalytic cycle. The liberated zinc species **E** serves as a Lewis acid again to be deactivated as zinc dibromide complex **F**, which was characterized by XAS measurements (Supplementary Figs. 20 and 21).

We performed DFT calculations for each step of the zinc-mediated SMC reaction to elucidate the reaction mechanism using 4-fluorobromobenzene (**1**) and potassium phenyl(trifluoro)borate (**2a**) as a model compound (Fig. 6 and Supplementary Figs. 23–26). The dissociation of one equivalent of amphos to afford **A** is endergonic with a considerable energy difference (Gibbs energy,  $\Delta G = +28.4 \text{ kcal mol}^{-1}$ ). After coordination of **1** to form **II**, oxidative

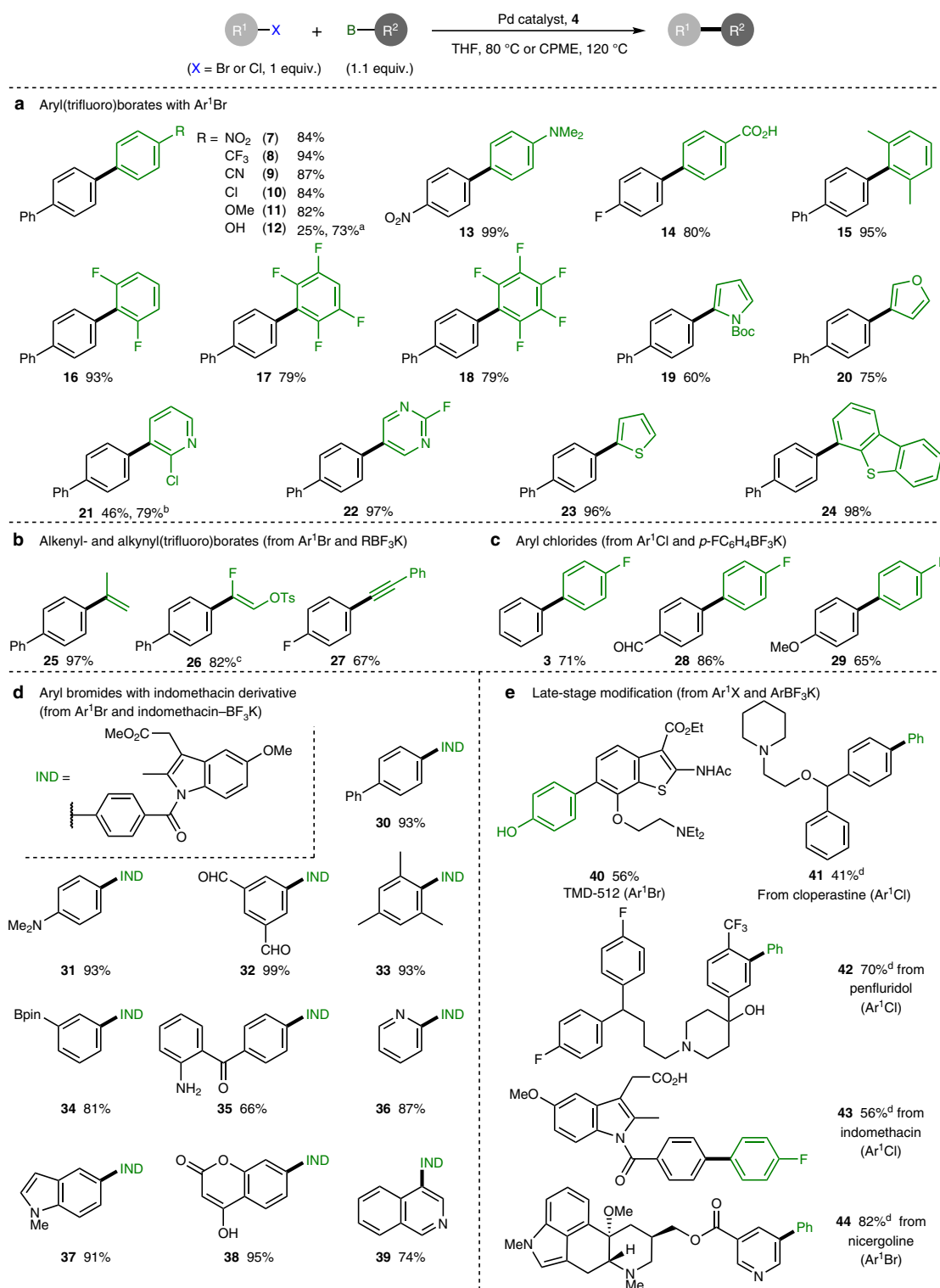


**Fig. 7 | Substrate scope.** Reaction conditions for ArBr (0.200 mmol, 1 equiv.): potassium organo(trifluoro)borate (1.1 equiv.), PdCl<sub>2</sub>(amphos)<sub>2</sub> (0.02 equiv.), **4** (0.78 equiv. per Zn), THF (1 ml), 80 °C, 3–24 h. Reaction conditions for ArCl (0.200 mmol, 1 equiv.): organoboron (1.1 equiv.), (cod)Pd(CH<sub>2</sub>TMS)<sub>2</sub> (0.04 equiv.), XPhos (0.1 equiv.), **4** (0.78 equiv. per Zn), CPME (1 ml), 120 °C, 3–6 h. Isolated yields are shown. Moieties drawn in black and green are derived from organohalides and organoborons, respectively. **a**, Scope of potassium aryl(trifluoro)borates. **b**, Reaction with potassium alkenyl- and alkynyl(trifluoro)borates. **c**, Reactions with aryl chlorides. **d**, Synthesis of indomethacin methyl ester derivatives with various aryl bromides. **e**, Late-stage modification of bioactive compounds. <sup>a</sup>An arylboronic acid (1.5 equiv.) was used instead of a potassium aryl(trifluoro)borate. <sup>b</sup>A 0.05 equiv. of PdCl<sub>2</sub>(amphos)<sub>2</sub> was used. <sup>c</sup>A 1 mmol scale. <sup>d</sup>A 0.1 mmol scale.

addition follows to afford aryl(bromo)palladium monomer **B**, which would be in equilibrium with dimer **5a** (+7.4 kcal mol<sup>-1</sup>). Debromination and dehydroxylation of **B** would afford **6**. Under

the stoichiometric conditions (Fig. 3), remaining **C** could abstract the hydroxy group as four equivalents of **4** were used for the quantitative conversion (Fig. 6, red). Although this step to produce **6**-OTf

is endergonic (+9.0 kcal mol<sup>-1</sup>), the (tmeda)Zn(OH)<sub>2</sub> by-product would oligomerize and precipitate out, making this process irreversible (Supplementary Fig. 24). Under the catalytic conditions, boron trifluoride (BF<sub>3</sub>), formed during both the initiation of the palladium catalyst and the transmetalation with **2a**, would be a preferable acceptor of the hydroxy group (blue). The dehydroxylation with BF<sub>3</sub> is favourable in Gibbs energy (-16.8 kcal mol<sup>-1</sup>) and proceeds to give **6**·BF<sub>3</sub>OH bearing hydroxy(trifluoro)borate as a counter anion. The following zinc removal process (**6**·BF<sub>3</sub>OH to **D** + **E**) was slightly endergonic (+5.8 kcal mol<sup>-1</sup>), supporting our hypothesis that transmetalation-active species **D** forms in equilibrium and predominantly exists as a relatively stable masked intermediate (**6**). The barrier for the transmetalation (**TS-2**) was estimated to be 20.7 kcal mol<sup>-1</sup>, which is consistent with the experimental result of the stoichiometric transmetalation without heating (Fig. 3). The following reductive elimination takes place smoothly via the transition state **TS-3** with an energy barrier of only 4.3 kcal mol<sup>-1</sup> to give **3** and regenerate **II**. Overall, this catalytic transformation is thermodynamically favourable. The highest energy barrier of the reaction, the ligand dissociation (**I** to **A** + amphos), is not too high. Indeed, the SMC reaction proceeds even at room temperature (Fig. 2a), supporting the theoretical results.

**Substrate scope.** The substrate scope of the zinc-mediated SMC reaction was explored mainly using aryl bromides and potassium aryl(trifluoro)borates. A broad range of aryl(trifluoro)borates with various substituents participated in the reaction to provide biaryls in high yields (Fig. 7a). The zinc-mediated conditions allowed the use of substrates with base-sensitive groups, including acidic functionals like phenolic (**12**, **38**) and carboxylic (**14**) moieties. Perfluorophenyl (**16**–**18**) and heteroaryl (**19**–**24**) substrates were found to be compatible with formation of the desired biaryls as well. Alkenyl- and alkynylborates, including a boryl(fluoro)alkene unit<sup>22</sup>, underwent the reaction smoothly to afford **25**–**27** (Fig. 7b). Our approach often showed a considerable efficiency compared to those of previously established methods, because the reactions with selected substrates under general conditions using potassium organo(trifluoro)borates<sup>23</sup> scarcely yielded products (Supplementary Table 19). When aryl chlorides were used as electrophiles, the desired products were not obtained under the standard conditions, despite the fact that the palladium catalysis with an amphos ligand is generally utilized for the SMC reaction with aryl chlorides<sup>24</sup>. We reoptimized the palladium catalyst and found that using a biaryl(dialkyl)phosphine was effective for the coupling reaction in the case of aryl chlorides (Fig. 7c and Supplementary Table 4). The robustness of the reaction to various functional groups prompted us to apply this method to the late-stage functionalization of bioactive compounds. The SMC reaction of indomethacin methyl ester with aryl bromides bearing various functional groups, such as diformyl, unprotected amino and coumarin moieties, proceeded uneventfully to provide the arylated products (**30**–**39**; Fig. 7d). Notably, we found that the (pinacolato) boryl group remained intact under our conditions, which indicated the potential application of this method for sequential coupling reactions<sup>25</sup>. The optimized conditions were also applicable to the synthesis or modification of bioactive compounds, such as TMD-512 (**40**)<sup>26</sup>, and the arylation of commercial medicines (**41**–**44**) bearing various functional groups, demonstrating the broad substrate scope of this method (Fig. 7e).

## Conclusions

In summary, we have established conditions for the SMC reaction of general organohalides with organoborons that do not require addition of a traditional base by using a zinc complex. The present method, involving the controlled release of a transmetalation-active organopalladium(II) species, allows the SMC reactions to occur without an external base and renders

substrates with base-sensitive moieties available, improving the synthetic utility. This approach, which controls the release of active species mediated by a Lewis acid, can innovate cross-coupling chemistry because transmetalation is a fundamental step in transition-metal-catalysed reactions. Furthermore, this concept can enhance the utility of chemical processes involving the generation of cationic organometallic intermediates, such as the electrophilic functionalization of carbon–hydrogen bonds<sup>27</sup> and polyolefin synthesis<sup>28</sup>, thus improving the efficiency of chemical production and lowering the environmental burden. Further investigations to explore Lewis acid catalysts for the base-independent SMC reaction and discover the scope of the controlled-release concept are currently underway.

## Methods

**General.** All reactions were performed in an argon atmosphere unless otherwise indicated. All manipulations of air- and/or moisture-sensitive compounds were performed either using standard Schlenk techniques or in a glovebox in an atmosphere of argon. Unless otherwise noted, zinc-mediated SMC reactions were conducted in a 4 ml (ø15 mm × 45 mm) screw-thread clear vial with a cap assembled with a septum. See the Supplementary Information for detailed conditions and the characterization data.

**Procedure for zinc-mediated SMC reaction with aryl bromides.** To a 4 ml capped vial equipped with a magnetic stir bar were added aryl bromide (0.200 mmol, 1 equiv.), organo(trifluoro)borate (0.220 mmol, 1.1 equiv.), PdCl<sub>2</sub>(amphos)<sub>2</sub> (2.8 mg, 4.0 μmol, 0.02 equiv.), **4** (54.2 mg, 0.156 mmol, 0.78 equiv. per Zn) and THF (1.0 ml). The mixture was stirred for the time indicated at 80 °C and then cooled to room temperature. The mixture was poured into saturated aqueous sodium hydrogen carbonate (~2 ml), and the mixture was extracted with EtOAc (~3 ml × 3). The combined organic extract was dried over Na<sub>2</sub>SO<sub>4</sub>. After filtration, the filtrate was concentrated under reduced pressure. The residue was purified by silica-gel column chromatography to give the corresponding products. Further purification was conducted with gel permeation chromatography (GPC) or high-performance liquid chromatography (HPLC) when required.

**Procedure for zinc-mediated SMC reaction with aryl chlorides.** To a 4 ml capped vial equipped with a magnetic stir bar were added aryl chloride (0.200 mmol, 1 equiv.), potassium aryl(trifluoro)borate (0.220 mmol, 1.1 equiv.), (cod)Pd(CH<sub>2</sub>TMS)<sub>2</sub> (3.1 mg, 8.0 μmol, 0.04 equiv.), 2-dicyclohexylphosphino-2',4',6'-triisopropyl-1,1'-biphenyl (XPhos, 9.5 mg, 20 μmol, 0.1 equiv.), **4** (54.2 mg, 0.156 mmol, 0.78 equiv. per Zn) and cyclopentyl methyl ether (CPME; 1.0 ml). The mixture was stirred for the time indicated at 120 °C and then cooled to room temperature. The mixture was poured into saturated aqueous sodium hydrogen carbonate (~2 ml), and the mixture was extracted with EtOAc (~3 ml × 3). The combined organic extract was dried over Na<sub>2</sub>SO<sub>4</sub>. After filtration, the filtrate was concentrated under reduced pressure. The residue was purified by silica-gel column chromatography to give the corresponding products. Further purification was conducted with GPC or HPLC when required.

## Data availability

The main data are available in the main text or the Supplementary Information. Data for the X-ray crystal structures of **4** and **5a** are available free of charge from the Cambridge Crystallographic Data Centre (<https://www.ccdc.cam.ac.uk/structures/>) under reference numbers CCDC 2073815 and CCDC 2073816, respectively. All other data are available from the authors upon reasonable request.

Received: 13 May 2021; Accepted: 2 November 2021;  
Published online: 17 December 2021

## References

- Miyaura, N. & Suzuki, A. Palladium-catalyzed cross-coupling reactions of organoboron compounds. *Chem. Rev.* **95**, 2457–2483 (1995).
- Schneider, N. et al. Big data from pharmaceutical patents: a computational analysis of medicinal chemists' bread and butter. *J. Med. Chem.* **59**, 4385–4402 (2016).
- Lennox, A. J. J. & Lloyd-Jones, G. C. Transmetalation in the Suzuki–Miyaura coupling: the fork in the trail. *Angew. Chem. Int. Ed.* **52**, 7362–7370 (2013).
- Cox, P. A. et al. Base-catalyzed aryl-B(OH)<sub>2</sub> protodeboronation revisited: from concerted proton transfer to liberation of a transient aryl anion. *J. Am. Chem. Soc.* **139**, 13156–13165 (2017).
- Cox, P. A., Leach, A. G., Campbell, A. D. & Lloyd-Jones, G. C. Protodeboronation of heteroaromatic, vinyl, and cyclopropyl boronic acids: pH-rate profiles, autocatalysis, and disproportionation. *J. Am. Chem. Soc.* **138**, 9145–9157 (2016).



6. Suzuki, A. Cross-coupling reactions of organoboranes: an easy way to construct C–C bonds (Nobel lecture). *Angew. Chem. Int. Ed.* **50**, 6722–6737 (2011).
7. Lennox, A. J. J. & Lloyd-Jones, G. C. Selection of boron reagents for Suzuki–Miyaura coupling. *Chem. Soc. Rev.* **43**, 412–443 (2014).
8. Valente, C. & Organ, M. G. in *Boronic Acids* Vol. 2 (ed. Hall, D. G.) Ch. 4 (Wiley, 2011).
9. Cammidge, A. N. et al. Aryl trihydroxyborates: easily isolated discrete species convenient for direct application in coupling reactions. *Org. Lett.* **8**, 4071–4047 (2006).
10. Yamamoto, Y., Takizawa, M., Yu, X.-Q. & Miyaura, N. Cyclic triolborates: air- and water-stable ate complexes of organoboronic acids. *Angew. Chem. Int. Ed.* **47**, 928–931 (2008).
11. Malapit, C. A., Bour, J. R., Brigham, C. E. & Sanford, M. S. Base-free nickel-catalyzed decarbonylative Suzuki–Miyaura coupling of acid fluorides. *Nature* **563**, 100–104 (2018).
12. Darses, S. et al. Cross-coupling of arenediazonium tetrafluoroborates with arylboronic acids catalyzed by palladium. *Tetrahedron Lett.* **37**, 3857–3860 (1996).
13. Chen, L., Sanchez, D. R., Zhang, B. & Carrow, B. P. “Cationic” Suzuki–Miyaura coupling with acutely base-sensitive boronic acids. *J. Am. Chem. Soc.* **139**, 12418–12421 (2017).
14. Chen, L., Francis, H. & Carrow, B. P. An “on-cycle” precatalyst enables room-temperature polyfluoroarylation using sensitive boronic acids. *ACS Catal.* **8**, 2989–2994 (2018).
15. Sanhueza, I. A. et al. Base-free cross-coupling of aryl diazonium salts in methanol: Pd<sup>II</sup>-alkoxy as reactivity-controlling intermediate. *Angew. Chem. Int. Ed.* **60**, 7007–7012 (2021).
16. Molander, G. A. & Jean-Gérard, L. in *Boronic Acids* Vol. 2 (ed. Hall, D. G.) Ch. 11 (Wiley, 2011).
17. Gillis, E. P. & Burke, M. D. A simple and modular strategy for small molecule synthesis: iterative Suzuki–Miyaura coupling of B-protected haloboronic acid building blocks. *J. Am. Chem. Soc.* **129**, 6716–6717 (2007).
18. Noguchi, H., Hojo, K. & Suginome, M. Boron-masking strategy for the selective synthesis of oligoarenes via iterative Suzuki–Miyaura coupling. *J. Am. Chem. Soc.* **129**, 758–759 (2007).
19. Zabinsky, S. I. et al. Multiple-scattering calculations of X-ray-absorption spectra. *Phys. Rev. B* **52**, 2995–3009 (1995).
20. Johnson, E. R. et al. Revealing noncovalent interactions. *J. Am. Chem. Soc.* **132**, 6498–6506 (2010).
21. Bader, R. F. W. Atoms in molecules. *Acc. Chem. Res.* **18**, 9–15 (1985).
22. Isoda, M. et al. Convergent synthesis of fluoroalkenes using a dual-reactive unit. *J. Org. Chem.* **86**, 1622–1632 (2021).
23. Molander, G. A., Canturk, B. & Kennedy, L. E. Scope of the Suzuki–Miyaura cross-coupling reactions of potassium heteroaryltrifluoroborates. *J. Org. Chem.* **74**, 973–980 (2009).
24. Guram, A. S. et al. New catalysts for Suzuki–Miyaura coupling reactions of heteroatom-substituted heteroaryl chlorides. *J. Org. Chem.* **72**, 5104–5112 (2007).
25. Lehmann, J. W., Blair, D. J. & Burke, M. D. Towards the generalized iterative synthesis of small molecules. *Nat. Rev. Chem.* **2**, 0115 (2018).
26. Shimizu, S., Hosoya, T., Murohashi, M. & Yoshida, S. Benzothiophene compound, alternative autophagy-inducing agent and anticancer drug including benzothiophene compound as active ingredient, and method for screening for compounds having anticancer activity. European patent, EP 2813226 (2013).
27. Gensch, T., Hopkinson, M. N., Glorius, F. & Wencel-Delord, J. Mild metal-catalyzed C–H activation: examples and concepts. *Chem. Soc. Rev.* **45**, 2900–2936 (2016).
28. Chen, C. Designing catalysts for olefin polymerization and copolymerization: beyond electronic and steric tuning. *Nat. Rev. Chem.* **2**, 6–14 (2018).

## Acknowledgements

We thank T. Ritter (Max-Planck-Institut für Kohlenforschung, Germany) for valuable comments on a draught of the manuscript and T. Honma at the Japan Synchrotron Radiation Research Institute for support of XAS experiments in SPring-8. XAS measurements were performed at the BL14B2 of SPring-8 with the approval of the Japan Synchrotron Radiation Research Institute (proposal nos 2020A1732 and 2020A1871) and at the BL-12C of KEK under the approval of the Photon Factory Program Advisory Committee (proposal no. 2020G006). Theoretical studies were performed at RIKEN on Hokusai Big Waterfall (proposal no. Q20509) and Research Center for Computational Science, Okazaki, Japan. This research was supported by JSPS KAKENHI grant nos 20K05521 (Scientific Research (C); T.N.), 20K15279 (Early-Career Scientists; Y.U.) and 19K16332 (Early-Career Scientists; M.L.); the Japan Agency for Medical Research and Development under grant no. JP20am0101098 (Platform Project for Supporting Drug Discovery and Life Science Research, BINDS; T.N. and T.H.); a Research Grant from Hyogo Science and Technology Association (FY2021; T.N.); a Mitsubishi Gas Chemical Award in Synthetic Organic Chemistry, Japan (Y.U.); the Pioneering Project ‘Chemical Probe’ from RIKEN (T.H.); and RIKEN–Osaka University Science and Technology Hub Collaborative Research Program from RIKEN and Osaka University (T.N. and Y.U.).

## Author contributions

T.N. and Y.U. conceived and designed the experiments and prepared the manuscript. M.I. participated in preliminary experiments. T.N., T.T. and M.N. carried out the chemical reactions, analysed the data and characterized the products. Y.U. conducted XAS experiments and analysis. D.H. performed single crystal X-ray diffraction analysis. T.N. and Y.U. conducted computational studies. T.N., Y.U., H.S. and T.H. discussed the results and edited the manuscript.

## Competing interests

The authors declare no competing interests.

## Additional information


**Supplementary information** The online version contains supplementary material available at <https://doi.org/10.1038/s41929-021-00719-6>.

**Correspondence and requests for materials** should be addressed to Takashi Niwa or Yuta Uetake.

**Peer review information** *Nature Catalysis* thanks Bao Nguyen and the other, anonymous, reviewer(s) for their contribution to the peer review of this work.

**Reprints and permissions information** is available at [www.nature.com/reprints](http://www.nature.com/reprints).

**Publisher’s note** Springer Nature remains neutral with regard to jurisdictional claims in published maps and institutional affiliations.

 **Open Access** This article is licensed under a Creative Commons Attribution 4.0 International License, which permits use, sharing, adaptation, distribution and reproduction in any medium or format, as long as you give appropriate credit to the original author(s) and the source, provide a link to the Creative Commons license, and indicate if changes were made. The images or other third party material in this article are included in the article’s Creative Commons license, unless indicated otherwise in a credit line to the material. If material is not included in the article’s Creative Commons license and your intended use is not permitted by statutory regulation or exceeds the permitted use, you will need to obtain permission directly from the copyright holder. To view a copy of this license, visit <http://creativecommons.org/licenses/by/4.0/>.

© The Author(s) 2021